

Steady-State Analysis of DFIG for Wind Power Generation System Drive

Jihène Ben Alaya , Adel Khedher and Mohamed Faouzi Mimouni

Abstract— Wind energy has a key role to play in producing of clean and less expensive electrical energy. Researchers develop the necessary procedure to optimize and to control this energy. They are focused on the control of the wind energy conversion system based on double fed induction generator (DFIG). In this paper, a steady-state study of DFIG generation system allows knowing the static limits of the system like its behavior versus the amplitude and phase angle of the equivalent injected rotor voltage variations. According to results, a good coordination between both direct and quadratic components of the injected rotor voltage of the DFIG allows to found an optimal operation of DFIG. Based on the steady-state analysis, a nonlinear vector control based on the second approach of Lyapunov of the rotor side converter and a direct power control strategy with no need of dc-link voltage regulation of the grid side converter is presented. Simulation results show a good performance of the generation system under the proposed strategies.

Keywords— Generation system, double fed induction generator, wind turbine control, steady-state, non linear vector control, direct power control

I. INTRODUCTION

THE fossil energy depletion, the global warming, gas emissions (CH_4 , PFC , HFC , N_2O , SF_6 , $Methane$, CO_2), the acid rain... reinforce the idea of free polluted, economic and durable production of electrical energy. Renewable energy sources, especially the wind one, as a non polluting energy and less expensive, have a key role to play in solving of all this problems [1]. To optimize and to control this energy, various generators have been used. Doubly-fed induction generator (DFIG) is the most popular topology used in present wind turbine systems. Moreover, actually, with the advancement of the electrical power converter and the micro-electronics, new structures based on the variable speed control are more and more used [2]. The main advantages are that the variable speed gives a good solution to generate an electrical energy at constant frequency and at unity power factor operation [3,4].

J. Ben Alaya is with the Electrical Engineering Department, Monastir Engineering School (ENIM), Monastir-TUNISIA
(corresponding author e-mail: bnajihene@yahoo.fr).

A. Khedher is with the Electrical Engineering Department, Sousse Engineering School (ENISo), Sousse-TUNISIA
(e-mail: adel_khedher@yahoo.fr).

M. F. Mimouni is with the Electrical Engineering Department, Monastir Engineering School (ENIM), Monastir-TUNISIA
(e-mail: mfmimouni@enim.rnu.tn).

Commonly, the DFIG is directly connected to the electrical network by the stator windings and through a bidirectional converter in the rotor windings. Such configuration offers several advantageous like the possibilities of active and reactive power control at hypynchronous and hypersynchronous generator operation mode and the decrease of the stresses on the mechanical structure. Furthermore, the power converters are rated for approximately 25% of the total exchanged power [5]. Various control strategies are developed in the literature to control the power converters of such WECS [5-10]. In this paper, a steady-state study of DFIG generation system allows knowing the static limits of the system like its behavior versus the amplitude and phase angle of the equivalent injected rotor voltage variations is presented. Based on the steady-state DFIG analysis, a nonlinear vector control (NLVC) based on the second approach of Lyapunov of the rotor side converter (RSC) is presented. For the grid side converter (GSC), this paper presents a new Direct Power Control (DPC) strategy able to control the operation of the GSC with no need of dc-link voltage regulation, something that conducts to a more simple algorithm.

This paper is organized as follows: the second section presents a description of the variable speed DFIG generation system. The maximum wind power extraction process is presented in the third section. In the fourth section, we present the DFIG model. The steady-state study of the DFIG is presented in the fifth section. Simulation results allowing knowing the static limits of the system are presented and discussed. Based on the steady-state DFIG analysis, a nonlinear vector control based on the second approach of Lyapunov of the rotor side converter and the direct power control strategy of the grid side converter are presented in the sixth section. Simulation results are presented and discussed and we finish by a conclusion.

II. DESCRIPTION OF THE WIND ENERGY CONVERSION SYSTEM

The general structure of the studied WECS under consideration is given by figure 1. The system is composed by three-bladed wind turbine coupled to the rotor of the DFIG though a mechanical gearbox whose gear ratio G is chosen in order to set the generator shaft speed within a desired speed range, as follows:

$$\Omega_m = G \Omega_t \quad (1)$$

$$T_m = \frac{T_t}{G} \quad (2)$$

The DFIG will be connected to a rural grid directly by the stator and through a back to back converter by the rotor. The

power electronics equipment carries only a fraction of the total power (20–30%) injected to the grid which reduce the losses and the cost in the power electronics converters.

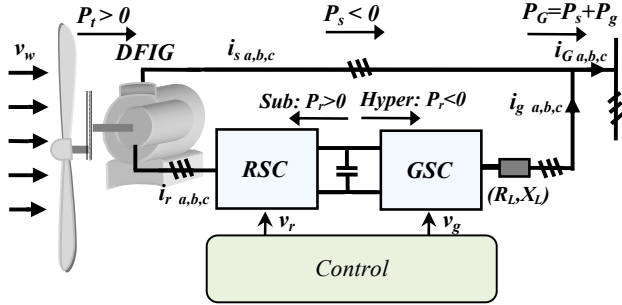


Fig. 1. Configuration of a DFIG wind turbine

III. WIND TURBINE POWER EXTRACTION

The mechanical power recovered by the wind turbine is expressed by [11,12]:

$$P_t = \frac{1}{2} \rho \pi R_b^2 C_p(\lambda, \beta) v_w^3 \quad (3)$$

where C_p is the turbine power coefficient which is function of the pitch angle of the rotor blades β and the tip speed ratio λ , defined as :

$$\lambda = \frac{\Omega_t R_b}{v_w} \quad (4)$$

The turbine power coefficient is expressed as:

$$C_p(\lambda, \beta) = 0.0174 (\beta - 2) \sin\left(\frac{\pi(\lambda + 0.1)}{14.34 - 0.3(\beta - 2)}\right) - 0.00092 (\lambda - 3) (\beta - 2) \quad (5)$$

The aerodynamic torque is then:

$$T_t = \frac{1}{2} \rho \pi R_b^3 C_q(\lambda, \beta) v_w^2 \quad (6)$$

Where:

$$C_q(\lambda, \beta) = \frac{C_p(\lambda, \beta)}{\lambda} \quad (7)$$

is the torque coefficient.

In this study, the pitch angle β remains unchanged and it's fixed to its optimal value.

In order to maximize wind power extraction, the rotor speed must be adjusted to track the optimal reference given by [5,13]:

$$\Omega_{opt} = \frac{\lambda_{opt} v_w}{R_b} \quad (8)$$

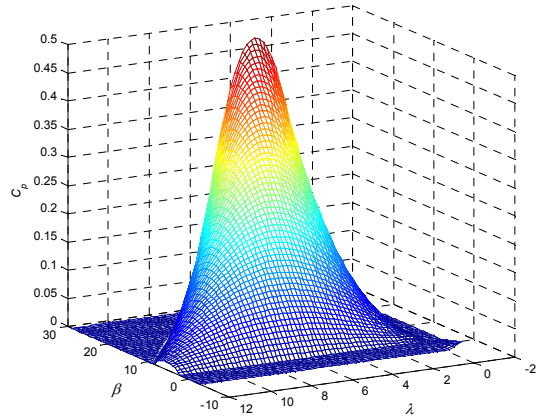


Fig. 2. Turbine power coefficient variations versus the pitch angle of the rotor blades and the tip speed ratio

In this study, the maximum power extraction process is realized. For each measured wind speed the rotational speed is varied to track the maximum power curve. The optimal mechanical power can be expressed as:

$$P_{t, opt} = \frac{1}{2} \rho \pi R_b^5 \frac{C_{p, max}}{\lambda_{opt}^3} \Omega_{opt}^3 \quad (9)$$

The simplified representation in the form of diagram blocks is given by figure 3.

For a given turbine type, the optimum power produced by the turbine vs. electrical speed is given by the following equation:

$$\begin{cases} P_t = 0.081\omega^3 + 5.1\omega^2 - 1.310^2\omega + 3.410^4 & \text{if } v_w < 25\text{m/s} \\ P_t = 3.4\text{MW} & \text{if } v_w \geq 25\text{m/s} \end{cases} \quad (10)$$

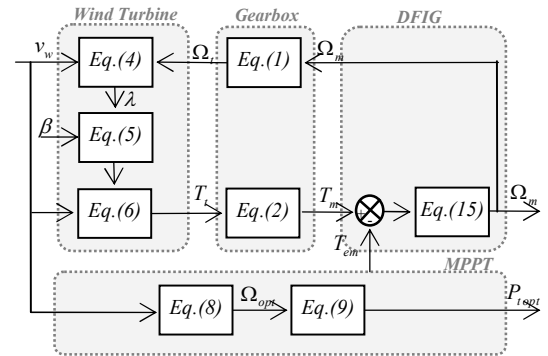


Fig. 3. Dynamic model scheme of the WECS

IV. DOUBLE FED INDUCTION GENERATOR MODEL

The voltage relations on rotor and stator sides are obtained by Kirchhoff's and Faraday's law as follows [5]:

$$\begin{cases} \vec{v}_s^s = R_s \vec{i}_s^s + \frac{d\vec{\varphi}_s^s}{dt} \\ \vec{v}_r^r = R_r \vec{i}_r^r + \frac{d\vec{\varphi}_r^r}{dt} \end{cases} \quad (11)$$

The instantaneous space vectors of stator and rotor voltages are written in the Park reference frame (d,q) as follows:

$$\begin{cases} \vec{v}_{s_dq} = R_s \vec{i}_{s_dq} + \frac{d\vec{\varphi}_{s_dq}}{dt} + j\omega_s \vec{\varphi}_{s_dq} \\ \vec{v}_{r_dq} = R_r \vec{i}_{r_dq} + \frac{d\vec{\varphi}_{r_dq}}{dt} + j\omega_r \vec{\varphi}_{r_dq} \end{cases} \quad (12)$$

The stator and rotor flux can be expressed as:

$$\begin{cases} \vec{\varphi}_{s_dq} = L_s \vec{i}_{s_dq} + L_m \vec{i}_{r_dq} \\ \vec{\varphi}_{r_dq} = L_m \vec{i}_{s_dq} + L_r \vec{i}_{r_dq} \end{cases} \quad (13)$$

With:

$$\begin{aligned} L_s &= L_{ls} + L_m \\ L_r &= L_{lr} + L_m \end{aligned}$$

The electromagnetic torque developed by the DFIG is given by the following:

$$T_{em} = \frac{3}{2} p M \Im m(\vec{i}_s^* \vec{i}_r) \quad (14)$$

The DFIG mechanical equation is derived from Park model expressed in a reference frame d - q rotating at synchronous speed ω_s as follows [8].

$$\left(\frac{J}{G^2} + J_m \right) \frac{d\Omega_m}{dt} + f\Omega_m = T_m - T_{em} \quad (15)$$

The DFIM equations derived from Park model given by (12,14), can be expressed using rotor and stator flux as follows:

$$\begin{cases} \frac{d\vec{\varphi}_s}{dt} = -f_{ss}\vec{\varphi}_s + f_{sr}\vec{\varphi}_r + \vec{v}_s \\ \frac{d\vec{\varphi}_r}{dt} = f_{rs}\vec{\varphi}_s - f_{rr}\vec{\varphi}_r + \vec{v}_r \\ T_{em} = \frac{p L_m}{\sigma L_s L_r} \Im m(\vec{\varphi}_s \vec{\varphi}_r^*) \end{cases} \quad (16)$$

With:

$$f_{ss} = \frac{1}{\sigma \tau_s} + j\omega_s ;$$

$$f_{sr} = \frac{L_m}{\sigma \tau_s L_r} ;$$

$$f_{rs} = \frac{L_m}{\sigma \tau_r L_s} ;$$

$$f_{rr} = \frac{1}{\sigma \tau_r} + j\omega_r$$

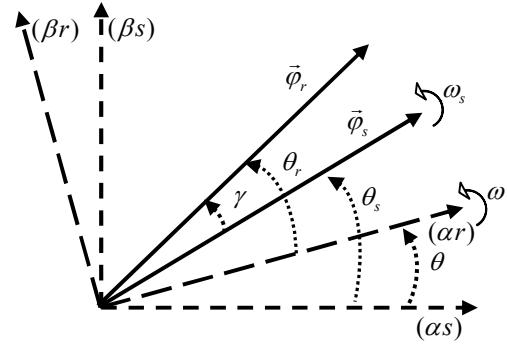


Fig. 4. Vector diagram of the DFIG variables

V. DFIG STADY-STATE ANALYSIS

A. DFIG Steady-State Model

In this part, the steady state approach is developed to study the behaviour of WECS. Under the steady-state condition and considering $\omega_r = s\omega_s$, the steady-state space vectors of stator and rotor voltages can be expressed from (12) and (13) as:

$$\begin{cases} \vec{v}_{s_dq} = R_s \vec{i}_{s_dq} + j\omega_s L_{ls} \vec{i}_{s_dq} + j\omega_s L_m (\vec{i}_{s_dq} + \vec{i}_{r_dq}) \\ \vec{v}_{r_dq} = \frac{R_r}{s} \vec{i}_{r_dq} + j\omega_s L_{lr} \vec{i}_{r_dq} + j\omega_s L_m (\vec{i}_{s_dq} + \vec{i}_{r_dq}) \end{cases} \quad (17)$$

The d - q steady-state equivalent circuit is obtained from (9) as shown by Figure 5.

The analytical equations derived from this classical model are used to compute the generator performances.

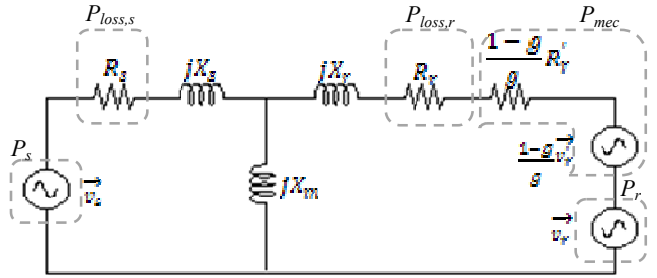


Fig. 5. Doubly-fed induction machine steady-state model

On the other hand, the stator active and reactive powers of the machine can be calculated directly from the stator voltage and currents as follows:

$$P_s = \frac{3}{2} (v_{sd} i_{sd} + v_{sq} i_{sq}) \quad (18)$$

$$Q_s = \frac{3}{2} (v_{sq} i_{sd} - v_{sd} i_{sq}) \quad (19)$$

By substituting the system (13) in the system (18) and by considering δ the angle between the rotor and stator flux vectors., the stator active and reactive power can be expressed in terms of stator and rotor flux vectors as follows:

$$\begin{cases} P_s = \frac{3}{2} \frac{L_m}{\sigma L_s L_r} \omega_s |\vec{\varphi}_s| |\vec{\varphi}_r| \sin \delta \\ Q_s = \frac{3}{2} \frac{\omega_s}{\sigma L_s} |\vec{\varphi}_s| \left(\frac{L_m}{L_r} |\vec{\varphi}_s| - |\vec{\varphi}_r| \cos \delta \right) \end{cases} \quad (20)$$

The active and reactive rotor powers are given by:

$$\begin{cases} P_r = \frac{3}{2} (v_{rd} i_{rd} + v_{rq} i_{rq}) \\ Q_r = \frac{3}{2} (v_{rq} i_{rd} - v_{rd} i_{rq}) \end{cases} \quad (21)$$

The losses powers in the stator and rotor windings are given by:

$$\begin{cases} P_{loss,s} = \frac{3}{2} R_s (i_{sd}^2 + i_{sq}^2) \\ P_{loss,r} = \frac{3}{2} R_r (i_{rd}^2 + i_{rq}^2) \end{cases} \quad (22)$$

B. DFIG Steady-State Simulation Results

Unlike a traditional induction machine, the DFIG operating characteristics not only depend on the applied stator voltage, but also depend on the injected rotor voltage. For simulation, the direct and quadratic components of the injected rotor voltage are defined as proportional to the stator voltage and are varied to observe the effect of variation in the active and reactive powers, the copper losses, the electromagnetic torque, the power factor and the fluxes characteristics. The behaviour of DFIG is presented as different characteristic curves. The simulation study is conducted by keeping the value of either V_{rd} or V_{rq} component constant while varying the other one. So, simulation analysis is performed to study the DFIG operating characteristics at different rotor voltage operation: solid line(-): $V_{rq}=0$; dotted line(·): $V_{rq}=0.1V_s$; dashed line(--): $V_{rq}=0.2V_s$. The parameters of the studied DFIG are given in appendix.

Figure (6) shows the performance of the stator active power (6.a), the stator reactive power (6.b), the rotor active power (6.c), the rotor reactive power (6.d), the stator copper losses (6.e) and the rotor copper losses (6.f) versus slip. Figure (7) shows the performance of the stator flux (7.a) and the rotor flux (7.b) versus slip. Figure (8) shows the performance of the electromagnetic torque vs. p.u. speed. Figure (9) shows the performance of the power factor vs. slip at different rotor voltage operation.

The power and the operating slip of a DFIG are affected by the amplitude and phase angle of the equivalent injected rotor voltage. Consequently, DFIG behaviors are different from induction machine having a short-circuited rotor. We remark that:

- When both direct and quadratic components of the injected rotor voltage are 0 (blue solid lines curves), the DFIG characteristic curves are the same as the induction machine characteristic having a short circuited rotor. The DFIM operates in generating mode only above the synchronous speed. There is no power output from the rotor of the

induction machine. The rotor power under both generator and motor modes are rotor copper loss.

- The DFIG rotor power is smaller than the DFIG stator power and the difference between the two really depends on the V_{rd} and V_{rq} values and the slip.

- The increase of V_{rd} from 0 to $0.2V_s$ while V_{rq} is kept constant at 0 (solid lines curves) or $0.1V_s$ (dotted lines curves) or $0.2V_s$ (dashed lines curves) shifts DFIG torque and active power characteristics to its generating mode. For both motoring and generating modes, the DFIG sends an additional active power through its rotor to the grid. The copper losses increase

- When increasing V_{rq} while keeping V_{rd} constant the DFIG operating speed shifts to a subsynchronous speed for its generating mode.

So, a good control and coordination between both direct and quadratic components of the injected rotor voltage of the DFIG is essential to prevent high currents flowing in the rotor and to found an optimal operation of DFIG in terms of torque, fluxes, active and reactive powers.

VI. POWER CONVERTER CONTROL

Based on the steady-state DFIG analysis, a nonlinear vector control using the second approach of Lyapunov of the rotor side converter and a direct power control strategy based on hysteresis controllers without any control loop of the grid side converter is developed.

A. Non Linear vector control strategy of the RSC

For large generator, we can neglect the effect of stator resistance face the stator voltage and magneto-motive force. So, in a Park reference frame linked to the stator flux, the stator voltage vector is consequently in quadratic advance with the stator flux vector. for each value of stator flux we can control the stator active and reactive powers by the quadrature and the direct rotor currents respectively [10,14].

The stability study of the system is based on the definition of a candidate function V which convergence towards zero constitutes the principle stability condition of the system. In this study, one considers a function of Lyapunov, definite positive, which minimizes the energy criterion, as follows:

$$\begin{aligned} V &= \frac{1}{2} (P_s - P_{sref})^2 + \frac{1}{2} (Q_s - Q_{sref})^2 \\ &= \frac{1}{2} (\Delta P_s)^2 + \frac{1}{2} (\Delta Q_s)^2 \end{aligned} \quad (23)$$

The reference powers are specified in order to extract the maximum power from wind energy for a given wind speed and to operate at unity power factor. The reference active power is given by:

$$P_{sref} = P_{tmax} - P_{loss,s} - P_{loss,r} \quad (24)$$

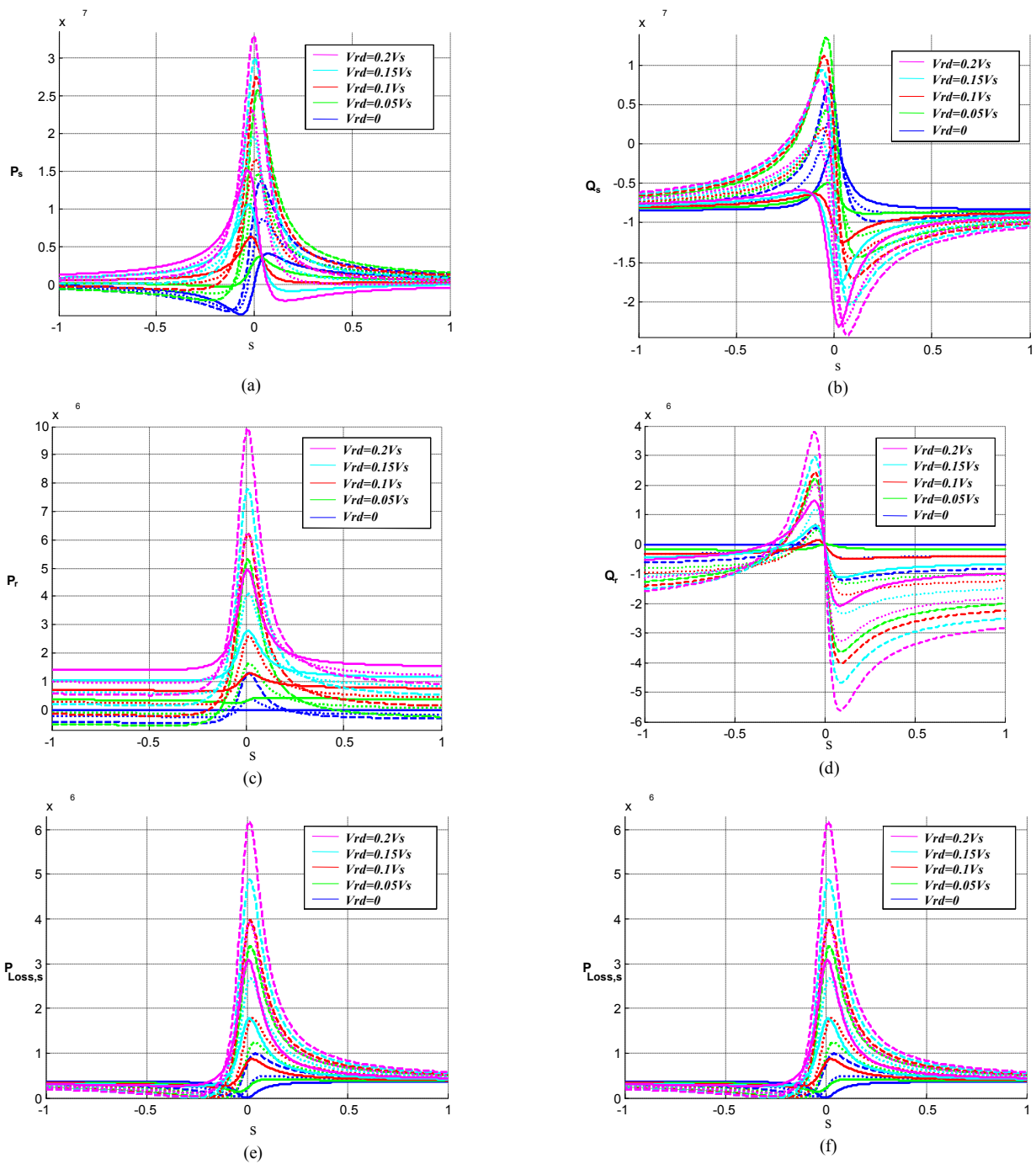


Fig. 6. Performance of the stator active power (a), stator reactive power (b), rotor active power (c), rotor reactive power (d), stator copper losses (e) and the rotor copper losses (f) vs. slip at different rotor voltage operation

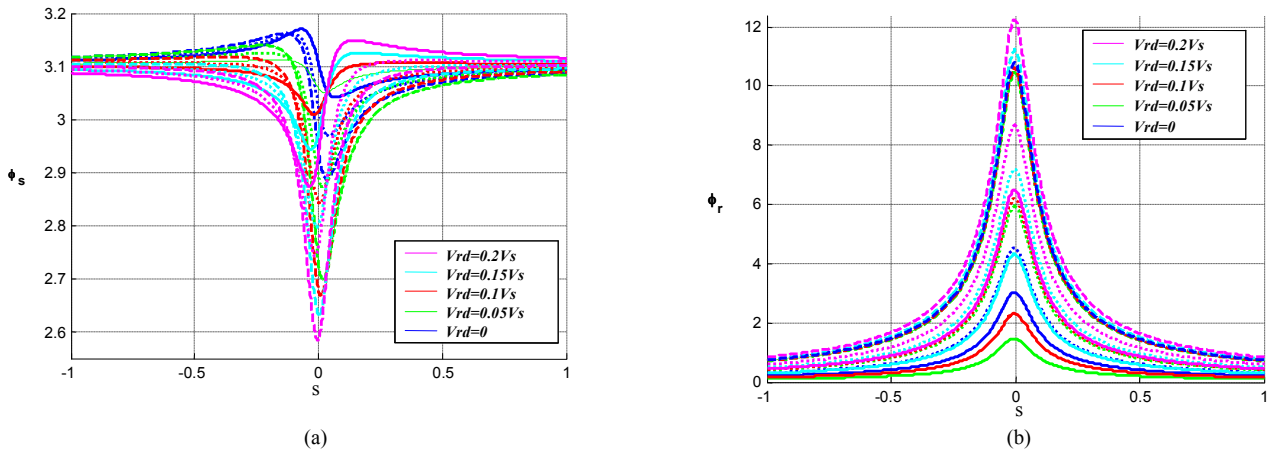


Fig. 7. Performance of the stator flux (a) and the rotor flux (b) vs. slip at different rotor voltage operation

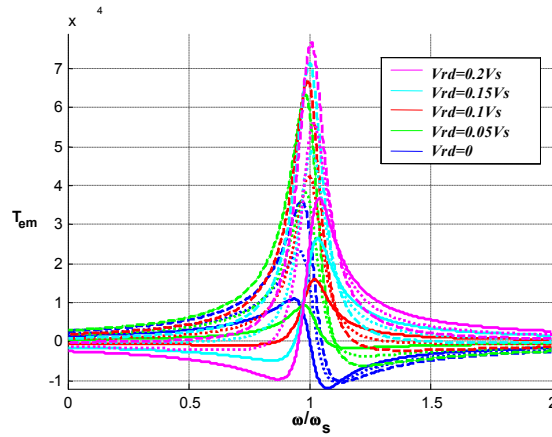


Fig.8. Performance of the electromagnetic torque vs. p.u. speed at different rotor voltage operation

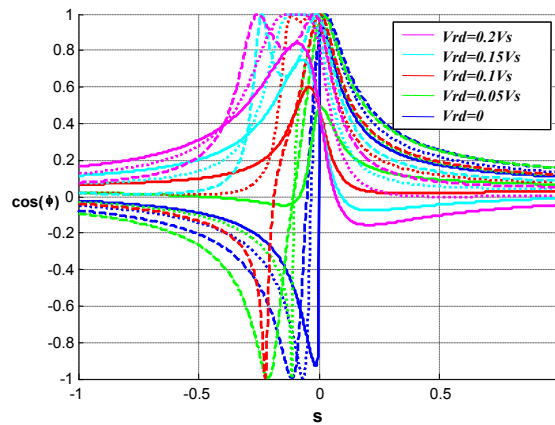


Fig.9. Performance of the power factor vs. Slip at different rotor voltage operation

According to Lyapunov theory the system is stable if the derivative of V is definite negative. We consider that:

$$\begin{cases} f_1 = \Re(-f_{ss} \bar{\varphi}_s + f_{sr} \bar{\varphi}_r) \\ f_2 = \Im(-f_{ss} \bar{\varphi}_s + f_{sr} \bar{\varphi}_r) \\ f_3 = \Re(f_{sr} \bar{\varphi}_s - f_{rr} \bar{\varphi}_r) \\ f_4 = \Im(f_{rs} \bar{\varphi}_s - f_{rr} \bar{\varphi}_r) \end{cases} \quad (25)$$

By applying the hypothesis of orientation of flux and of voltage to the systems (16) the derivative of Lyapunov function becomes:

$$\begin{aligned} \dot{V} = \Delta P_s \left[\frac{-3M}{2\sigma L_s L_r} v_{sq} (f_4 + v_{rq}) - \dot{P}_{sref} \right] \\ + \Delta Q_s \left[\left(\frac{3v_{sq}}{2\sigma L_s} f_1 - \frac{3M}{2\sigma L_s L_r} v_{sq} (f_3 + v_{rd}) \right) - \dot{Q}_{sref} \right] \end{aligned} \quad (26)$$

Knowing that to satisfy the energy criterion the derivative of Lyapunov function must be definite negative, one defines then two numbers K_1 and K_2 strictly positive, such as:

$$\dot{V} = -K_p (P_s - P_{sref})^2 - K_q (Q_s - Q_{sref})^2 \quad (27)$$

With:

$$\begin{cases} K_p \geq \frac{1}{\Delta P_s} \left[\frac{3M}{2\sigma L_s L_r} v_{sq} (f_4 + v_{rq}) + \dot{P}_{sref} \right] \\ K_q \geq \frac{1}{\Delta Q_s} \left[\frac{-3v_{sq}}{2\sigma L_s} f_1 + \frac{3M}{2\sigma L_s L_r} v_{sq} (f_3 + v_{rd}) + \dot{Q}_{sref} \right] \end{cases} \quad (28)$$

the control voltages of RSC are consequently expressed as follows:

$$\begin{cases} v_{rd} = \frac{2\sigma L_s L_r}{3M v_{sq}} \left(\frac{3}{2\sigma L_s} f_1 v_{sq} - \frac{3M}{2\sigma L_s L_r} f_3 v_{sq} - \dot{Q}_{sref} + K_q \Delta Q_s \right) \\ v_{rq} = \frac{2\sigma L_s L_r}{3M v_{sq}} \left(-\frac{3M}{2\sigma L_s L_r} f_4 v_{sq} - \dot{P}_{sref} + K_p \Delta P_s \right) \end{cases} \quad (29)$$

The control broad of the rotor side converter is illustrated by figure 10.

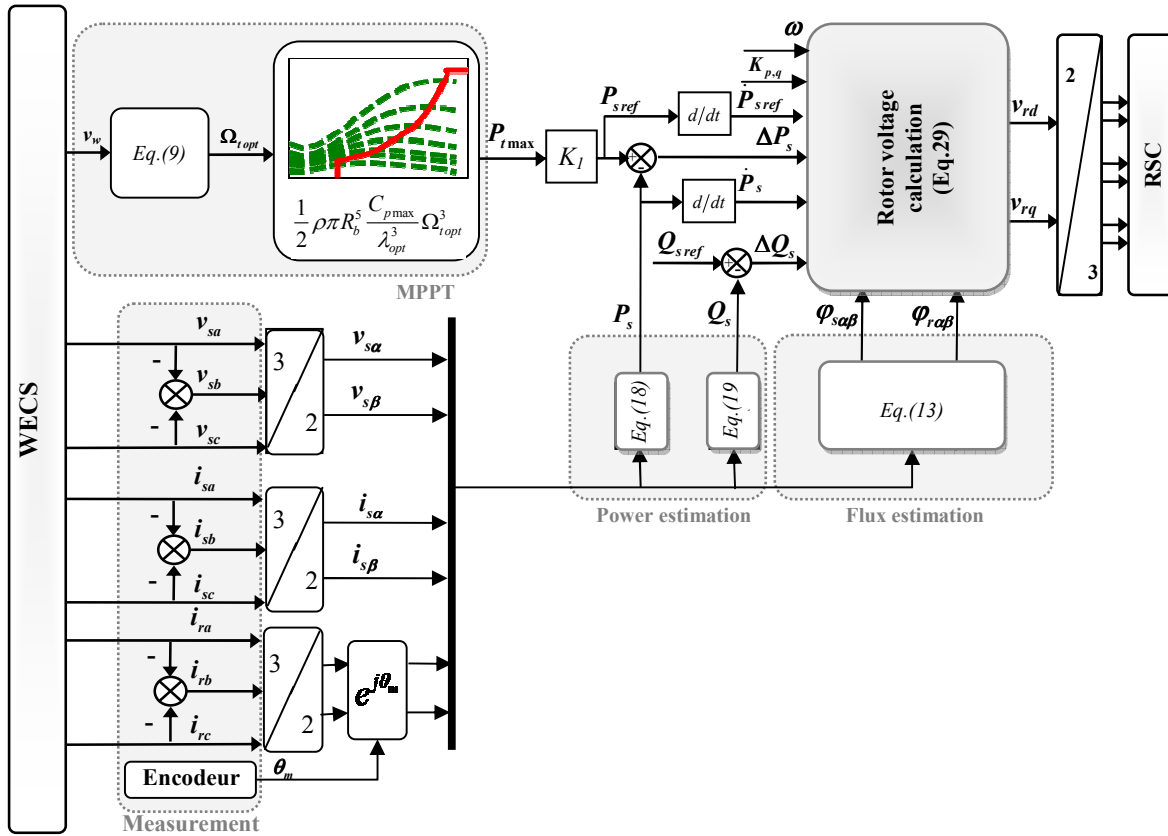


Fig. 10. Non Linear Vector Control Structure of the RSC

B. Direct Power Control Strategy of the GSC

The GSC is equipped by a two-stage controller operating in a grid AC voltage reference frame. It controls the power flow exchange with the grid via the rotor. The GSC current output is determinate by Kirchhoff laws applied at the connection between the grid and the wind generator system.

The proposed DPC strategy is constructed around two hysteresis controllers that allow grid injected power regulation [15,16]. The DPC controls the grid voltage vector and this by controlling the active and reactive power P_g and Q_g estimated from the following relations:

$$\begin{cases} P_g = \frac{3}{2} (v_{Gd} i_{gd} + v_{Gq} i_{gq}) \\ Q_g = \frac{3}{2} (v_{Gq} i_{gd} - v_{Gd} i_{gq}) \end{cases} \quad (30)$$

To select the optimum converter terminal voltage vector, one must know the relative position of the virtual grid flux in the six sextants as shown in figure 11.

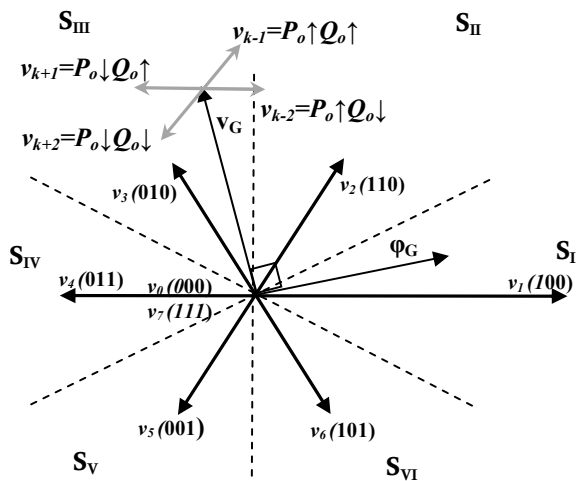


Fig.11 Effect of converter terminal voltage vector on the active and reactive powers

The structure of the direct power control is illustrated by figure 12. To calculate the reference GSC powers and to operate at unity power factor, we have neglected the losses powers in the stator, in the rotor and in the dc-bus.

C. Simulation Results of the WECS

Simulations results are made by using the real parameters of a wind turbine AE43 and a DFIG rated at 660KW and 690V. We notice that the wind variation has influence on the location of system operation mode. The proposed maximum power point tracking (MPPT) strategy associated to NLVC and DPC strategies are able to follow the wind speed changes rapidly. As it can be seen, the speed converges to its reference value rapidly.

The proposed approaches allows a quick stator flux response to be achieved these are justified by the directly connection of the stator to the grid.

The rotor flux is affected by wind variations. Indeed, as we can show an increase of wind, respectively a decrease; introduce an increase, respectively a decrease, of the rotor flux, which produce a sudden change in the electromagnetic torque, the transient's active power and the current injected to the grid.

With the NLVC strategy applied to the RSC and the DPC applied to the GSC, we remark firstly that the SPF converge to -1, this confirm the null-VAR operation mode. Secondly, the currents in the three phase's network constitute a balanced system of the rural network frequency.

VII. CONCLUSION

In this paper, the maximum wind power extraction process was illustrated. A steady-states analysis of a DFIG was presented. The stator and rotor powers, copper losses, fluxes and power factor are analyzed versus slip for different injected rotor voltage. From simulation results, we have concluded that a good coordination between both direct and quadratic components of the injected rotor voltage of the DFIG is essential to found an optimal operation of DFIG. Based on the steady-state DFIG analysis, a nonlinear vector control (NLVC) was developed to control the RSC. For the GSC, this paper have presents a new Direct Power Control (DPC) strategy able to control the operation of the GSC with no need of dc-link voltage regulation, something that conducts to a more simple algorithm. Simulation have shown that the developed control strategies allows a null-VAR operation mode and the generation of balanced system currents at the rural network frequency.

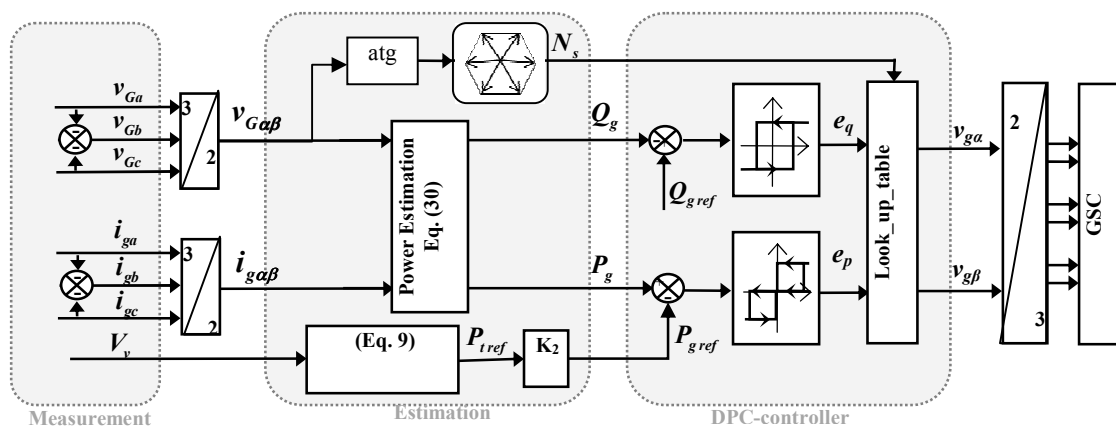


Fig.12. DPC strategy block diagram of GSC

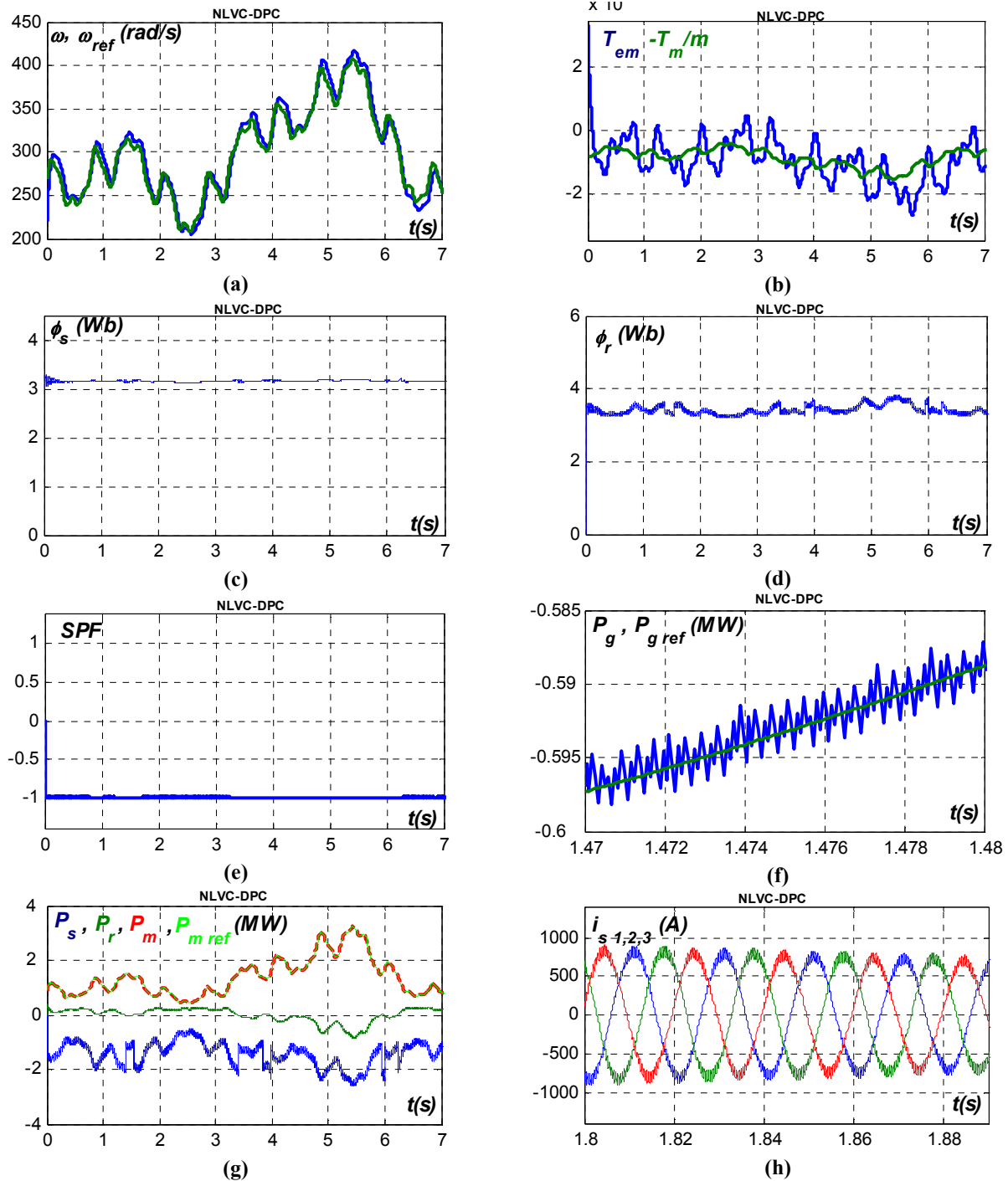


Fig. 13. DFIG Generation System Response:

(a) $\omega - \omega_{ref}$, (b) T_{em} , (c) ϕ_s , (d) ϕ_r , (e) SPF , (f) $P_g, P_{g ref}$, (g) $P_s, P_r, P_m, P_{m ref}$, (h) I_{s1}, I_{s2}, I_{s3}

APPENDIX

Induction generator data

Rated power: 660 Kw,

Rated stator voltage: 400/690V, 50Hz,

$R_r=0.0238 \Omega$, $R_s=0.0146 \Omega$,

$L_s=0.0306 H$, $L_r=0.0303H$, $L_m=0.0299H$,

$J_m=28 kg.m^2$, Number of pair poles: $p=2$,

Damping coefficient: $f=26$

Wind turbine data

Number of blades=3, Rotor diameter: $2R_b=43.5m$,
 Gearbox coefficient: $G = 55.747$,
 Cut-in wind speed: $v_{min}=3m/s$,
 Cutoff wind speed: $v_{max}=25m/s$,
 Optimal tip speed ratio: $\lambda_{opt}=8$,
 Moment of inertia: $J=238 kg.m^2$.

Power coefficient expression

$$C_p = \sum_{i=0}^5 a_i \lambda^i$$

With:

$$a_5=-0.000373, a_4=0.009309,$$

$$a_3=-0.081857, a_2=0.2774,$$

$$a_1=-0.19084, a_0=0.021945.$$

Grid parameters

Network rated voltage: $v_G=975V, 50Hz$,
 $R_L=3\Omega$,
 $L_L=0.051H$.

REFERENCES

- [1] Rohrig, K.; Lange, B. "Improvement of the Power System Reliability by Prediction of Wind Power Generation". *Power Engineering Society General Meeting, IEEE*. 24-28. pp.1 – 8. June 2007
- [2] Blaabjerg, F. ; Chen, Z., "Power Electronics for Modern Wind Turbines" Synthesis Lectures on Power Electronics, 2006
- [3] Y. Tang, L. Xu, "A flexible active and reactive power control strategy for a variable speed constant frequency generating system", *IEEE Transactions On Power Electronics*, 10(4): 472 -478. 1996.
- [4] Liu Qihui, He Yikang, Zhang Jianhua, "Operation control and modeling & simulation of AC-excited variable-speed constant-frequency (AEVSCF) wind power generator", *Proceeding of the CSEE*, 2006, 26(5):43 50.
- [5] J. Ben Alaya, A. Khedher and M.F. Mimouni. "Variable Speed Vector Control Strategy of the Double Fed Induction Generator Integrated in Electrical Grid," *International Conference on Ecologic Vehicles and Renewable Energy (EVER '08)*, Monaco, France. March 2008.
- [6] S. Drid, M^{ed} S. Nait-Said, A. Makouf and M^{ed} Tadjine. "Doubly Fed Induction Generator Modeling and Scalar Controlled for Supplying an Isolated Site", *Journal of Electrical Systems*. vol.2, no. 2. pp. 103-115. 2006.
- [7] M. Salles, J.R. Cardoso, A.P. Grilo, C. Rahmann and K. Hameyer. "Control strategies of doubly fed induction generators to support grid voltage," *IEEE International Conference on Electric Machines and Drives (IEMDC'09)*. pp.1551–1556. 3-6 May 2009.
- [8] C. Belfedal, S. Moreau, G. Champenois, T. Allaoui and M. Denai. "Comparison of PI and Direct Power Control with SVM of Doubly Fed Induction Generator," *Journal of Electrical and Electronics Engineering*. vol.8, no.2. pp. 633-641. 2008.
- [9] M. Rahimi and M. Parniani. "Dynamic behavior analysis of doubly-fed induction generator wind turbines, The influence of rotor and speed controller parameters," *International Journal of Electrical Power and Energy Systems*. Vol.32, Issue 5. pp. 464–477. June 2010.
- [10] J. Ben Alaya, A. Khedher, M.F. Mimouni. DTC and Non Linear Vector Control Strategies applied to the DFIG operated at Variable Speed, WSEAS Transactions On Environment And Development, Issue 11, Vol. 6, pp744-754, November 2010
- [11] H. Cheng, Y. Hou, and F. Wu, "Probabilistic Wind Power Generation Model: Derivation And Applications", *International Journal Of Energy (IJE)*, pp.17-26, Issue 2, Vol. 5, 2011
- [12] J. Sargolzaei and A. Kianifar, "Estimation of the power ratio and torque in wind turbine Savonius rotors using artificial neural networks", *International Journal Of Energy (IJE)*, pp.33-50, Issue 2, Vol. 1, 2007
- [13] Qingrong Zeng; Liuchen Chang; Riming Shao. "Fuzzy-logic-based maximum power point tracking strategy for Pmsg variable-speed wind turbine generation systems". *Canadian Conference on Electrical and Computer Engineering. CCECE 2008*. pp.405–410. 4-7 May 2008.
- [14] V.G. Rau and G. Durga Prasad. "Dynamic stability assessment of wind turbine generators using the Lyapunov function approach," *Electric Power Systems Research*. vol.27, no.1. pp. 61-72. May 1993.
- [15] L. Xu, D. Zhi, and L.Y. Liao "Direct Power Control of Grid Connected Voltage Source Converters", *Proc. IEEE PES GM*, 2007.
- [16] Dawei Zhi; Lie Xu; Williams, B.W. "Improved direct power control of three-phase PWM converters". *Industrial Electronics, 2008. IECON 2008. 34th Annual Conference of IEEE*. pp.778-783. 10-13 Nov. 2008.

J. Ben Alaya was born in Sousse, Tunisia in 1981. She received the engineering and Master degrees from the Engineering School of Monastir, in 2005 and 2007, respectively. She is registered in Ph.D. in Electrical Engineering in Monastir engineering school (ENIM). From 2005 to 2007, she has been a training teacher in the professional training center of Sousse-Tunisia. From 2007 to 2010, she has been an assistant professor in the Electric Engineering Department of High School of Sciences and Technologie (ESST-HS)-Tunisia. From November 2010, she is a Learning Councilor in the professional training center of M'Saken-Tunisia. Her main research interests are in the area of DFIG Drive, Power Electronics, Wind Power Generation Systems, and Renewable Energy.

A. Khedher received the Ph.D and University habilitation degrees in Electrical Engineering at Sfax-Tunisia in 2005 and 2012 respectively. He is currently a Professor in Electrical Engineering Department in Sousse engineering school (ENISo)-Tunisia. His specific research interests are in the area of Power Electronics, Motors Drives, Renewable Energy, Wind Power Generation Systems, ...

M.F. Mimouni received the Ph.D and University habilitation degrees in Electrical Engineering Department at Monastir-Tunisia in 1997 and 2004 respectively. He is currently a Professor in Electrical Engineering Department of Monastir Engineering School (ENIM). His specific research interests are in the area of Power Electronics, Motors Drives, Renewable Energy, Wind Power Generation Systems, ...